# Development of Compact Proton Synchrotron for Radiation Therapy

K. Endo, K. Egawa and Z. Fang

KEK
1-1 Oho, Tsukuba-shi, Ibaragi-ken, 305-0801 JAPAN

Abstract The present status of the magnet and power supply systems for a compact medical proton synchrotron under development is described according to experiences obtained from the detailed field measurement on the prototype 3T dipole magnet and the full scale 200 kA pulsed power supply. By sacrificing the small momentum dispersion of the original lattice, it is possible to achieve the smaller synchrotron ring with the reduced number of the quadrupole magnet keeping the present specification of the dipole. Based on the design studies for the compact proton synchrotron some prospects are given on the design of the compact carbon-ion synchrotron.

## 1. Introduction

As for the development of the compact 200 MeV proton synchrotron for the radiotherapy, a prototype 3 T dipole magnet was manufactured and its field quality was measured with the 200 kA pulsed power supply which was developed within the scope of this project [1]. The power supply was modified last year to excite all dipoles of the synchrotron ring and its performance was confirmed. The RF system including a compact RF cavity loaded with the magnetic alloy cores and a wideband RF power supply will be ready soon. In this fiscal year both dipole and quadrupole magnets will be manufactured to satisfy the minimum requirement to test the synchrotron performance such as the tracking between the dipole and quadrupole field and between the dipole field and the RF frequency.

For the beam optics with missing quardupoles, a new magnet configuration will be applied to achieve a stable betatron oscillation under a limited momentum spread allowance and an increased momentum dispersion. However, it is still useful to confirm the performance and to foresee the feasibility of the compact proton synchrotron.

## 2. Dipole Magnet Design and Performance

The ring consists of 4 dipole magnets. One of them shown in Fig.1 was manufactured as a prototype and its field quality was measured precisely. The aperture of the dipole is relatively large compared to the design at BINP [2] to attain the momentum aperture of ±1.5% according to the original lattice design [3]. Its cross-section is given in Fig.2. As shown in Fig.3 two types of unit core block made of the 0.5 mm thick laminations of Si-steel, 7 unit core blocks of 11.25 deg. and 2 half-unit core blocks of 5.625 deg., were assembled to form one dipole magnet. The short core blocks was placed at both ends of the dipole in order to machine the pole surface to have the tapered shape to maintain the almost constant effective length up to the maximum excitation level. The core block was heat-treated to glue the laminations coated with epoxy resin. Welding method was not used to avoid the core deformation. The finished core blocks were machined and assembled in the steel fixture to form a 90 deg sector as shown in Fig.2. Parameters of the dipole magnet are given in Table1.

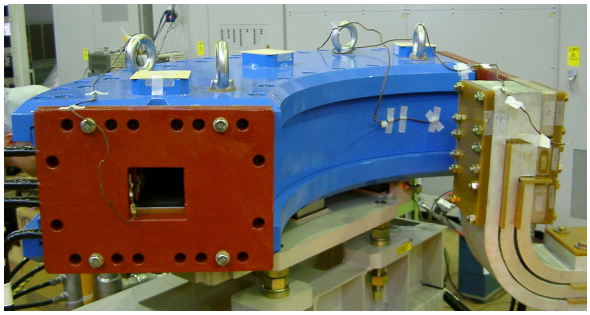

Figure 1: Prototype of the dipole magnet.

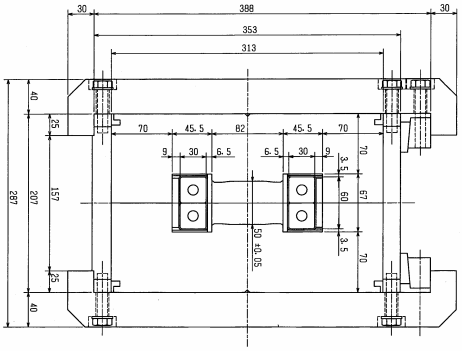


Figure 2: Cross-sectional dimensions of the dipole.

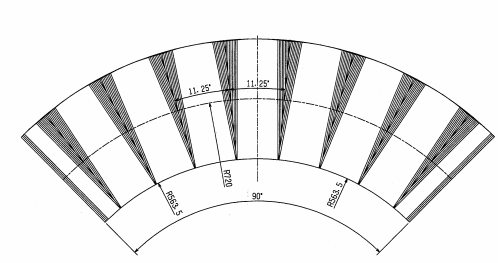


Figure 3: Assembled laminated 7 unit core and 2 half-unit core blocks.

Coil was made of the two Cu strand cables with the cross-section of 30 x 30 mm$^2$ which were welded to the Cu plates with the water cooling channels at the both magnet ends to make a single turn. One of the problems of this structure is the temperature rise because of the large resistivity and small heat conductivity. It allows only 1 Hz repetition rate for the rise of ΔT~80 deg.

Table 1: Dipole magnet parameters.

| | Proton ring | Carbon-ion ring |
|---|---|---|
| Peak current (kA) | 200 | 270 |
| Max. field (T) | 3 | 4 |
| Magnet length (m) | 1.13 | 2.12 |
| Bending radius (m) | 0.72 | 1.35 |
| Number of magnet | 4 | 4 |
| Coil turn number | 1 | 1 |
| Number of cooling circuits | 2 | 2 |

The field distribution was measured with the radially aligned 15 search coils of Fig.4 assembled on the girder shown in Fig. 5. They are moved manually at every 0.9 or 0.45 deg. step on the girder. Induced voltage was saved at every 2 μsec and integrated to convert it to the magnetic field. The normalized distribution measured at the center of the dipole magnet is shown in Fig.6 with the results of the numerical 3D dynamic field simulation.

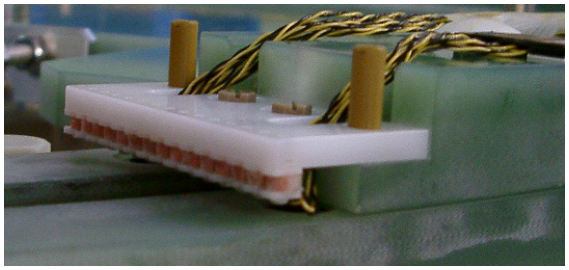

Figure 4: Search coils for the field measurement.

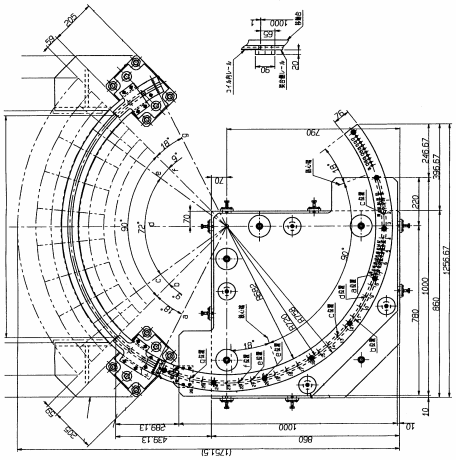

Figure 5: Field measuring girder. Dipole is left side.

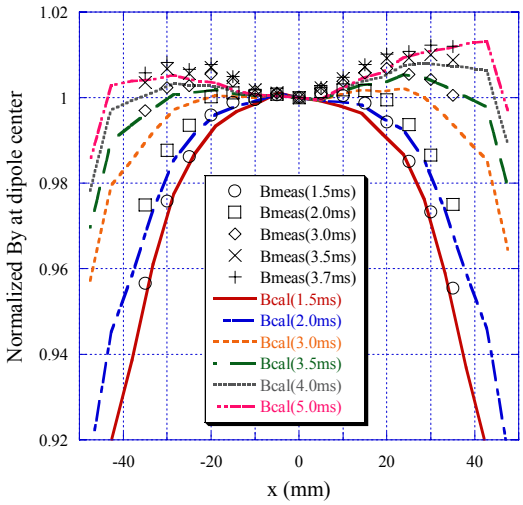


Figure 6: Normalized field distribution at the dipole center, Bmeas and Bcal mean the measured and calculated field distribution, respectively.

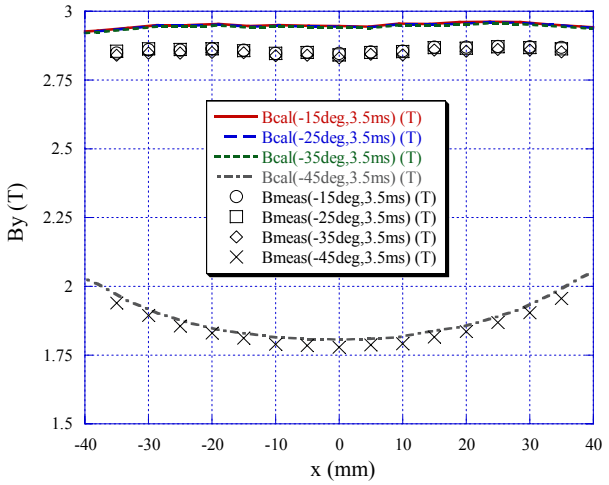


Figure 7: Measured and calculated radial field distributions at the different angular positions (-50<θ<0 deg.) at 3.5 msec. The -45 deg. is at an edge of the dipole magnet.

Comparing the numerical result with the calculated distribution, the 3D dynamic simulation predicts well the performance of the dynamic field distribution of the prototype dipole magnet. Large sextupole error field will be compensated with the correction windings and separate sextupole magnets. Comparisons are also made at the different angular positions as shown in Fig.7.

To make the effective magnet length independent of the excitation level, several cases in Fig.8 to the pole end profile were numerically simulated and the calculated results are given in Fig.9 with the measured data.

The adopted pole end profile is cases 80 and 81 in Fig.8, but the measured effective length is longer by 17 mm than calculation at low field side. It is not clear why the effective length decreases rapidly when the central field approaches to 3 T.

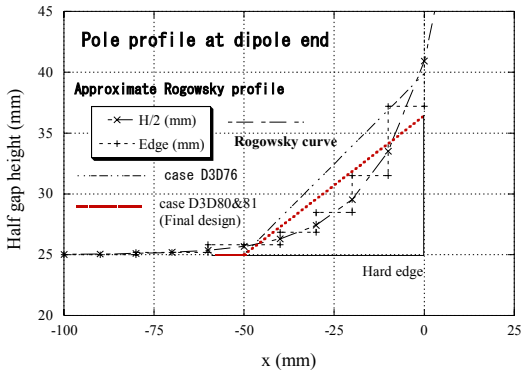


Figure 8: Pole profile at the dipole end.

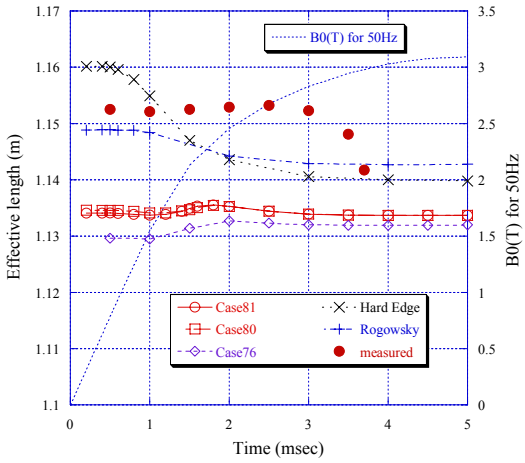


Figure 9: Calculated and measured effective length along the central orbit (R=0.72 m). Cases 80 and 81 are adopted for the prototype dipole magnet.

## 3. Quadrupole Magnet and New Lattice

The original lattice design requires large current for the excitation of the quadrupole magnets and their power supply system requires a large budget. To reduce these requirements it is decided to reduce the number of the quadrupoles and to find the new magnet configuration allowing the space for the installation of the RF cavity and other components. The horizontal and vertical tunes depend on the length of the straight section. As a result the circumference becomes 9.5 m instead of 11.9 m for the original lattice. Fig.10 is the new lattice parameters using 4 defocusing quadrupoles with the peak field gradient of 5 T/m at 200 MeV. The lattice parameters also depend on the strength of the quadrupoles. Especially the vertical tune dependence on the quadrupole strength is large as shown in Fig.11.

By reducing the circumference the RF frequency increases. Assuming the injection energy of 2 MeV, its range becomes 2.04 ~ 17.9 MHz. The momentum spread at injection increases to ±4.0% from the original design of ±3.2% and the momentum dispersion increase from 0.43 to 0.80. It is expected that the momentum aperture decreases from ±1.5% to ±1.0%.

A benefit obtained from new lattice is that the quadrupole parameters are mitigated because the maximum excitation level becomes lower.

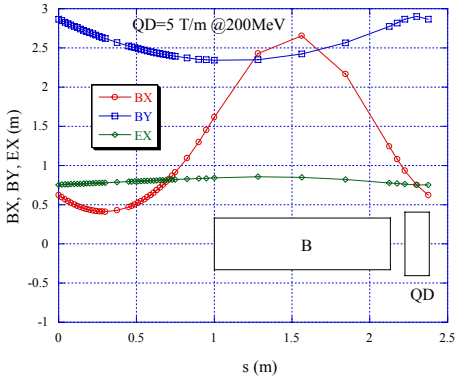


Figure 10: Lattice parameters using 4 defocusing quadrupoles with 5 T/m at 200 MeV. In this case tunes are 1.58 and 0.60 for horizontal and vertical direction, respectively.

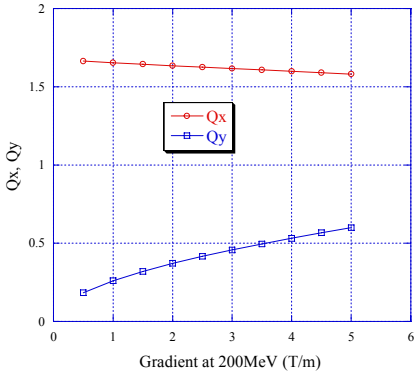


Figure 11: Tune dependence on the quadrupole strength.

## 4. Pulsed Power Supply of Dipole Magnet

As the dipole parameters do not changes even if the new lattice configuration is applied, there is no alteration to the 200 kA pulsed power supply (Fig.12) and an additional capacitor is installed to excite the serially connected all dipole magnets up to 3 T. The maximum energy storage of the capacitor amounts to about 200 kJ (10 mF). The peak dipole field or the peak beam energy is adjusted by changing the charge voltage of the capacitor because the peak current of the dipole magnet is determined by the capacitor voltage. So it is easy to change the beam energy from pulse to pulse.

The dipole magnet is excited by discharging the capacitor through the step-down pulse transformer of Fig.13 to increase the dipole current by the ratio of the primary to the secondary winding [4]. As the discharge current is hard to control except for the peak current, the tracking between the dipole and quadrupole field should be done by controlling the quadrupole magnet current.

The residual energy in the secondary circuit of the dipole magnets after finishing the acceleration is

recovered by switching the power switching elements from the discharge to the recovery mode and the dissipated energy is compensated by charging the capacitor to the specified voltage with the IGBT inverter. The output current and the dipole field are plotted in Fig.14 when the energy recovery circuit is working. The charge and discharge of the capacitor repeated during the synchrotron operation. The repetition rate is governed by both the temperature rise of the dipole magnet coil and the charging speed of the IGBT inverter.

Figure 12: Pulsed power supply equipped with an additional capacitor. Two separate pictures are merged at the middle.

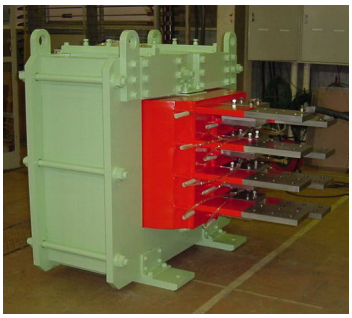

Figure 13: Step-down transformer.

## 5. Prospects to Compact Heavy Ion Synchrotron

Most significant component for the compact heavy ion synchrotron is the dipole magnet. Required beam aperture, which depends on the injection energy, determines the stored energy of the capacitor.

As lower injection energy requires larger aperture leading to larger stored energy. Extending the dipole design of the proton ring to the carbon ion synchrotron, the peak field will be 4 T at 300 MeV/u with the circumference of 16.5 m. Corresponding peak current is 270 kA maintaining the same beam aperture but the yoke width is larger than that of the proton ring to moderate the iron core saturation. The dipole parameters are also given in Table 1 and the numerical 3D dynamic field simulation gives the radial field distribution of Fig.15 at the center of the dipole. Large sextupole field component arises from the heavy saturation of the pole corners. Inductance is almost twice of the dipole of the proton ring requiring more capacitor unless the beam aperture is reduced by increasing injection energy and by reducing the saturation.

As the RF frequency range is narrower than the proton ring, the same RF cavity may be used, but the accelerating voltage becomes almost twice because of the small charge-to-mass ratio [5].

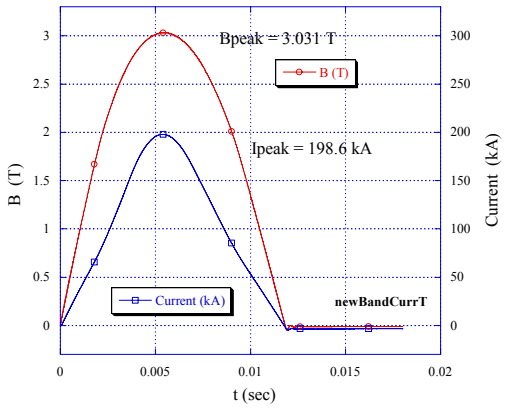


Figure 14: Current pulse and dipole field.

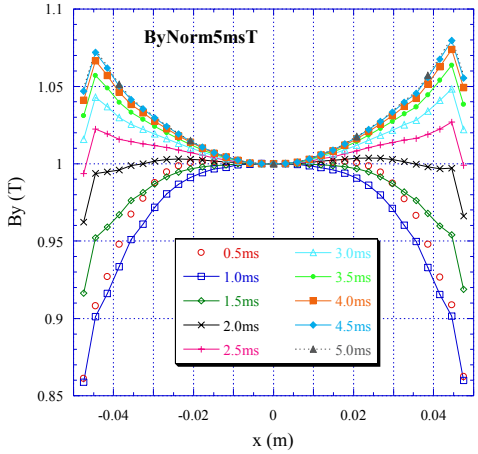


Figure 15: Radial field distribution at the dipole center at 4 T corresponding to 300 MeV/u.

## 6. References


[1] K. Endo et al, "Compact Proton and Carbon Ion Synchrotron for Radiation Therapy," Proc. EPAC2002, Paris, pp.2733-5.

[2] L. Picardi et al, "Preliminary Design of a Technologically Advanced and Compact Synchrotron for Proton Therapy," Internal Report RT/INN/94/20, 1994.

[3] K. Endo et al, "Development of High Field Dipole and High Current Pulse Power Supply for Compact Proton Synchrotron," Proc. PAC'03, Portland, to be published.

[4] K. Endo et al, "Resonant Pulse Power Supply for Compact Proton and/or Heavy Ion Synchrotron," Proc. APAC'01, Beijing, 2001, pp.636-8.

[5] K. Endo et al, "Compact Proton and Heavy Ion Synchrotron for Cancer Therapy and Bio-Science," Proc. 13th Symp. Acc. Sci. and Tech. Osaka, 2001, pp.426-8.